International Journal of Mechanical, Industrial and Aerospace Sciences
ISSN: 2517-9950
Vol:6, No:11, 2012

CFD Analysis of Incompressible Turbulent Swirling Flow through Circle Grids Space Filling Plate

B. Manshoor, M. Jaat, and Amir Khalid

***Abstract*—**Circle grid space filling plate is a flow conditioner with a fractal pattern and used to eliminate turbulence originating from pipe fittings in experimental fluid flow applications. In this paper, steady state, incompressible, swirling turbulent flow through circle grid space filling plate has been studied. The solution and the analysis were carried out using finite volume CFD solver FLUENT 6.2. Three turbulence models were used in the numerical investigation and their results were compared with the pressure drop correlation of BS EN ISO 5167-2:2003. The turbulence models investigated here are the standard k-ε, realizable k-ε, and the Reynolds Stress Model (RSM). The results showed that the RSM model gave the best agreement with the ISO pressure drop correlation. The effects of circle grids space filling plate thickness and Reynolds number on the flow characteristics have been investigated as well.

***Keywords*—**Flow conditioning, turbulent flow, turbulent modeling, CFD.

I. Introduction

FLOW measurement is essential in almost all industrial applications; from food industry to petrochemical, and oil/gas processing. In some applications, such as pharmaceutical plants, the high accuracy of flow metering is unrelentingly required in order to control the precise chemical reactions and drug formation processes. On the other hand, errors in flow measurement can result in huge cost losses and inefficiency repercussions. For instance, slight flow metering inaccuracies can cause enormous monetary losses in the transfer of oil and natural gas due to the great volumes involved in these transfers.

The installation conditions of flowmeters have a more pronounced effect on their performance than construction. Numerous research workers have investigated experimentally and computationally these effects with reference to the shift in flow meter discharge coefficient. Aichouni et al. [1, 2] reported errors up to ±30% on a Venturi flow meter while Yeh and Matingly [3] reported errors up to ±17% on an ultrasonic flow meter when the meter is subject to distorted flow conditions. Given that most industrial pipe fittings, which are sources of both swirl, asymmetries and turbulence distortions, ensuring that fully developed flow in terms of both mean flow and turbulence structure approaches the meter is difficult to achieve in practice. Another disadvantage of pipe fittings, in this sense, is the generation of distorted velocity profiles associated with varying degrees of swirl at the inlet of flowmeter. Satisfactory stipulations to avoid flowmeter calibration and measurement errors entail a flow with 2º swirl angle and a ratio of axial velocity at any point on a given pipe cross section to the maximum axial velocity at the same cross section is within 5% of the corresponding ratio of fully developed flow as measured in the same pipe after 100 pipe diameter length [4].

In order to achieve these conditions, great lengths of straight pipes are required between the flowmeter and the nearest upstream fitting to decay the vortical motion of the turbulent swirling flow; these lengths are typically equivalent to 600 times of the pipe diameter [5]. Large and costly upstream pipe assemblies are required to comply with these flow conditions in order to diminish the crucial articulated flow metering errors. Alternatively, turbulent swirling flow can be adapted to meet the conditions of flowmeter minimum-error performance by the employment of flow conditioners upstream of the flowmeter.

Flow conditioners are designed to reorder the velocity profile in order to create fully developed turbulent flow [6]. Although these devices have been used for decades, there are several questions that need to be answered to define the geometry that would provide the optimum performance. Such performance is characterized by minimum swirl angle, more stable and repetitive velocity profile as well as minimum downstream pipe length.

The circle grids space filling flow conditioner consists of a thin perforated plate with various holes diameters designed to eliminate swirl. The holes diameter is increasing towards the plate center with a fractal pattern. The smaller holes are designed near the plate edge in order to break down the swirl, which intensifies near the boundary. Its swirl-removing efficiency increases with plate thickness. Experimental works using this type of flow conditioner showed that the fractal flow conditioner located at 5D upstream of the orifice plate give the small change in discharge coefficient compare to the standard one [7]. The experiment was carried out for the range

B. Manshoor is a lecturer in the Faculty of Mechanical and Manufacturing Engineering, Universiti Tun Hussein Onn Malaysia, 86400 Pt Raja, Batu Pahat, Johor Malaysia (phone: +607-453-8404; fax: +607-453-6080; e-mail: bukhari@uthm.edu.my).

M. Jaat is a head of department in the University and Industry Relations Office, Universiti Tun Hussein Onn Malaysia, 86400 Pt Raja, Batu Pahat, Johor Malaysia (phone: +607-453-7193; fax: +607-453-6262; e-mail: norrizam@uthm.edu.my).

Amir Khalid is a senior lecturer in the Faculty of Mechanical and Manufacturing Engineering, Universiti Tun Hussein Onn Malaysia, 86400 Pt Raja, Batu Pahat, Johor Malaysia (phone: +607-453-8484; fax: +607-453-6080; e-mail: amirk@uthm.edu.my).

of Reynolds number 5000 to 75,000 and it can be concluded that this kind of fractal flow conditioner has positive effect on disturbed flow for low and high Reynolds number.

II. Objectives and Description

In this paper, the turbulent swirling flow through circle grid space filling plate is analyzed through three turbulence models in order to determine the most suitable models to simulate such flow problems. Moreover, the effect of plate thickness on the flow dynamics is studied numerically. A detailed flow insight is presented to explain the flow separation and recovery within the plate holes as well as visualizing the swirl removal effect of the circle grid space filling plate at different thicknesses. One purpose of this study is to determine the optimum plate thickness that would result in a swirl-free flow after the shortest distance downstream of the conditioner plate. The CAD geometry and numerical model are validated through a comparison between the pressure drops resulting from three turbulent models with the pressure drop calculated by standard equations. Subsequently, the pressure drop resulting from the selected turbulence model is validated with the standard pressure drop at four different flow rates. The validated turbulence model is used afterwards to study the effect of plate thickness on the flow dynamics.

III. Mathematical Formulation

A. Geometry of the Circle Grids Space Filling Plate

Circle grids space filling plate has two grades of holes, as described in Fig. 1 and Table I. The smaller holes are concentrated near the plate edge because the major concentration of eddies and swirl is near the wall. On the other hand, this radial reduction of hole diameter assists in stabilizing the velocity distribution. The geometry of holes is expressed in terms of plate diameter (i.e. pipe internal diameter). In the present study, an outer diameter of 50 mm is adopted for the circle grids space filling plate.

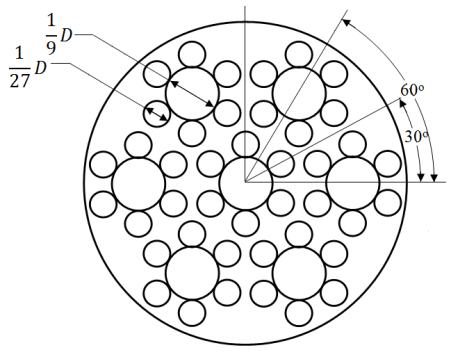

Fig. 1 Description of circle grids space filling flow conditioner plate

TABLE I
Details of Circle Grids Space Filling Flow Conditioner Plate Geometry

Hole grade	Number of holes	Hole diameter
1	7	0.111D ±0.002 D
2	42	0.037D ±0.002 D
Standard plate thickness		$0.12D \le t_p \le 0.15D$
Standard upstream pipe length		$17D \le L_f$
Standard downstream pipe length		$7.5D \le L_s \le L_f$ - 8.5D

B. Governing Equations

In this study, incompressible, unsteady, and isothermal flow is assumed. Based on these assumptions, the governing equations are as follows:

$$\frac{\partial}{\partial x_j}(\rho \bar{u}_i) = 0 \tag{1}$$

$$\frac{\partial}{\partial t}(\rho \bar{u}_j) + \frac{\partial}{\partial x_i}(\rho \bar{u}_i \bar{u}_j) = \frac{\partial}{\partial x_i}\left(\mu\left[\frac{\partial \bar{u}_i}{\partial x_j} + \frac{\partial \bar{u}_j}{\partial x_i}\right]\right) - \frac{\partial \bar{p}}{\partial x_j} + \rho g_j + \frac{\partial}{\partial x_i}\tau_{ij} \tag{2}$$

where u is the velocity component in x_i direction, ρ is the density and p is the static pressure. In the case of RANS modeling, the over-bar denotes time averaging. The stress tensor τ_{ij} is an unknown term representing Reynolds stress tensor ($\rho\overline{u_i' u_j'}$) in the case of RANS. This additional term in the governing equations is the result of averaging of time dependent Navier-Stokes equations and needs to be modeled in order to achieve closure. Details about transport equation and closure approximation are presented in reference [8].

C. Turbulence Modelling

In this section the three turbulence models used in the numerical simulation are described briefly.

The Standard k-ε Model. The standard *k-ε* model is a two equation eddy viscosity turbulence model [9]. In this model, the eddy viscosity is computed based on the turbulence kinetic energy *k*, and the turbulence dissipation rate *ε* via:

$$v_t = C_\mu \frac{k^2}{\varepsilon} \tag{3}$$

Each of these two turbulence scales has its transport equation. The turbulence kinetic energy equation is derived from the exact momentum equation by taking the trace of the Reynolds stress. This equation can be expressed as:

$$\frac{\partial k}{\partial t} + \bar{u}_i \frac{\partial k}{\partial x_i} = v_t\left[\frac{\partial \bar{u}_i}{\partial x_j} + \frac{\partial \bar{u}_j}{\partial x_i}\right]\frac{\partial \bar{u}_i}{\partial x_j} + \frac{\partial}{\partial x_i}\left(\frac{v_t}{\sigma_k}\frac{\partial k}{\partial x_i}\right) - \varepsilon \tag{4}$$

The dissipation rate equation, on the other hand, is obtained using physical reasoning. The equation is:

$$\frac{\partial \varepsilon}{\partial t} + \bar{u}_i \frac{\partial \varepsilon}{\partial x_i} = C_{\varepsilon 1} \frac{\varepsilon}{k} v_t \left[\frac{\partial \bar{u}_i}{\partial x_j} + \frac{\partial \bar{u}_j}{\partial x_i} \right] \frac{\partial \bar{u}_i}{\partial x_j} + \frac{\partial}{\partial x_i} \left(\frac{v_t}{\sigma_\varepsilon} \frac{\partial \varepsilon}{\partial x_i} \right) - C_{\varepsilon 2} \frac{\varepsilon^2}{k} \quad (5)$$

The standard k-ε has five empirical constants C_μ, σ_k, σ_ε, $C_{\varepsilon 1}$ and $C_{\varepsilon 2}$ with values of 0.09, 1.0, 1.3, 1.44 and 1.92, respectively. These values were obtained from experiments and computer optimization. It is worth noting that these values are not universal and the *k-ε* model requires a certain amount of fine tuning in order to obtain correct results.

The Realizable k-ε Model. Shih and coworkers have proposed a new k-ε model in order to improve the performance of the standard model [10]. In the new model, the eddy viscosity formulation satisfies the mathematical constraint of the positivity of the normal Reynolds stresses. This is achieved by making C_μ variable and sensitizing it to the mean flow (i.e. mean deformation) and the turbulence (i.e. *k* and *ε*). Moreover, the realizable *k-ε* model adopts a new transport equation for the dissipation rate which is based on the dynamic equation of the mean-square vorticity fluctuation. The new dissipation rate equation is:

$$\frac{\partial \varepsilon}{\partial t} + \bar{u}_i \frac{\partial \varepsilon}{\partial x_i} = C_{\varepsilon 1} S \varepsilon + \frac{\partial}{\partial x_i} \left(\frac{v_t}{\sigma_\varepsilon} \frac{\partial \varepsilon}{\partial x_i} \right) - C_{\varepsilon 2} \frac{\varepsilon^2}{k + \sqrt{v\varepsilon}} \quad (6)$$

The model constants σ_ε and $C_{\varepsilon 2}$ have values of 1.2 and 1.9 respectively while $C_{\varepsilon 1}$ is computed from:

$$C_{\varepsilon 1} = max \left[0.43 \frac{\left(S \frac{k}{\varepsilon} \right)}{\left(S \frac{k}{\varepsilon} \right) + 5} \right] \quad (7)$$

where, $S = \sqrt{2 S_{ij} S_{ij}}$ and $S_{ij} = \frac{1}{2} \left(\frac{\partial u_j}{\partial x_i} + \frac{\partial u_i}{\partial x_j} \right)$.

The eddy viscosity is computed as in the standard model via equation (3). However, in order to ensure the positivity of the normal Reynolds stresses C_μ is no longer a constant and it is computed from:

$$C_\mu = \frac{1}{A_o + A_s U^* \frac{k}{\varepsilon}} \quad (8)$$

where, $A_o = 4.0$, $U^* = \sqrt{S_{ij} S_{ij} \Omega_{ij} \Omega_{ij}}$,
$A_s = \sqrt{6} \cos \left(\frac{1}{3} \arccos \left(\sqrt{6} W \right) \right)$, $W = \frac{\sqrt{8} S_{ij} S_{jk} S_{ki}}{S^3}$
and vorticity tensor, $\Omega_{ij} = \frac{1}{2} \left(\frac{\partial \bar{u}_i}{\partial x_j} - \frac{\partial \bar{u}_j}{\partial x_i} \right)$.

The Reynolds Stress Model. The Reynolds stress model involves calculation of the individual Reynolds stresses $\bar{u}_i' \bar{u}_j'$ using differential transport equations [11, 12]. The individual Reynolds stresses are then used to obtain closure of the Reynolds-averaged momentum equation, thus, avoiding the use of the eddy viscosity approximation which was proven to perform poorly in many types of flows. The exact form of the Reynolds stress transport equations can be derived by taking moments of the exact momentum equation. This is a proces s wherein the exact momentum equations are multiplied by a fluctuating property, the product then being Reynolds-averaged stress. Unfortunately, several of the terms in the exact equation are unknown and modeling assumptions are required in order to close the equations.

The exact transport equations for the transport of the Reynolds stresses, is:

$$\frac{\partial}{\partial t} \left(\rho \overline{u_i' u_j'} \right) + \frac{\partial}{\partial x_k} \left(\rho u_k \overline{u_i' u_j'} \right) = - \frac{\partial}{\partial x_k} \left[\rho \overline{u_i' u_j' u_k'} + \overline{p \left(\delta_{kj} u_i' + \delta_{ik} u_j' \right)} \right] + \frac{\partial}{\partial x_k} \left[\mu \frac{\partial}{\partial x_k} \left(\overline{u_i' u_j'} \right) \right] - \rho \left(\overline{u_i' u_k'} \frac{\partial u_j}{\partial x_k} - \overline{u_j' u_k'} \frac{\partial u_i}{\partial x_k} \right) - \rho \beta \left(g_i \overline{u_j' \theta} + g_j \overline{u_i' \theta} \right) + \overline{p \left(\frac{\partial u_i}{\partial x_j} - \frac{\partial u_j}{\partial x_i} \right)} - 2 \mu \overline{\frac{\partial u_i}{\partial x_k} \frac{\partial u_j}{\partial x_k}} 2 \rho \Omega_k \left(\overline{u_j' u_m'} \varepsilon_{ikm} + \overline{u_i' u_m'} \varepsilon_{jkm} \right) \quad (9)$$

Some terms in these exact equations, namely the convection, molecular diffusion, stress production, and production by system rotation do not require any modeling. However, the turbulent diffusion, buoyancy production, pressure strain, and dissipation need to be modeled to close the equations. Many approximations have been made to close these equations [8].

IV. Simulation

A. CFD Model Description

For all the CFD models used in this study, except for flow insight, a cell size of 1mm^3 is used in the circle grid space filling plate region, and a size function is applied to the upstream and downstream flow regions. The size function has a growth rate of 1.25% with a maximum cell size of 3mm^3. The circle grid space filling plate region has 8214 cells, and the upstream and downstream flow regions have 326012 and 350544 cells respectively. The diameter and length of the cylindrical computational domain are 0.05m and 0.8m respectively. The boundary conditions used with the incompressible CFD model are constant velocity inlet and ambient pressure outlet. All walls are assumed to have no-slip boundary conditions.

B. CFD Model Validation

In order to validate the proposed CFD model, and select the optimum turbulence model to implement in the presented study, all the above mentioned models have been run. The inlet axial and swirl velocity components were 11.55 m/s and 6.1 m/s, respectively. It should be noted that at the inlet section of the computational domain, the axial and tangential velocities maintain constant values with respect to the radial direction up to the wall. The resultant pressure drop across the circle grids space filling flow conditioner plate was compared for the five turbulence models with the value calculated using

the standard equation in (ISO, 2003), which calculates the pressure drop as a function of the dynamic head:

$$\Delta P = K\frac{1}{2}\rho v^2 \quad (10)$$

where K is the coefficient of discharge, estimated at a value of 3 [4]. The standard pressure drop was calculated using equation (10), and it was found to be 238.5 Pa. In contrast, the pressure drop was computed from the CFD analysis, using different turbulence models, at distances 1D and 0.5D upstream and downstream the circle grid space filling plate, respectively. Table II gives the validation results.

TABLE II
PRESSURE DROP ACROSS THE CIRCLE GRIDS SPACE FILLING PLATE FOR THREE DIFFERENT TURBULENT MODELS

Turbulence model		CFD computed ΔP (Pa)	Deviation from standard ΔP
Standard k-ε	1st order	304.6	27.76%
	quick	279.2	17.11%
k-ε Realizable		261.3	9.61%
RSM		280.8	17.78 %

The results show that the standard k-ε models performed poorly in this type of flow, with the realizable k-ε performing slightly better than the RSM and the standard k-ε models. The unexpected superiority of the realizable k-ε over the RSM is justified by the inadequacy of implementing RSM for wall induced shear flows which are dominated by the small eddies. This requires the grid size to be reduced substantially in order to have a successful RSM computation.

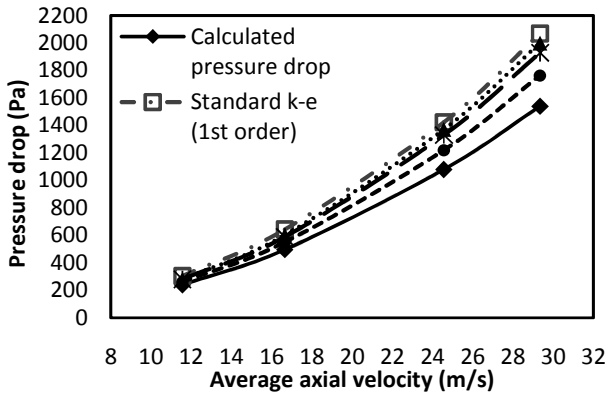

Fig. 2 Comparison between standard and simulated pressure drops across circle grids space filling plate at four different axial velocities

Subsequently pressure drop was computed across the circle grids space filling flow conditioner at four different axial velocities with a constant inlet swirl angle of 20°. The purpose of this stage of validation is to confirm the suitability of all models to solve the present problem. The computed pressure drop is plotted against the average inlet axial velocity in Fig. 2.

V. Results and Discussion

The effect of plate thickness on eliminating swirl from the flow field is explained in terms of two parameters: tangential velocity and swirl angle. Figure 3 illustrates the planar velocity vectors at inlet and outlet sections for the circle grids space filling flow conditioner with four different thicknesses. The swirl angle at the inlet is constant at 20°.

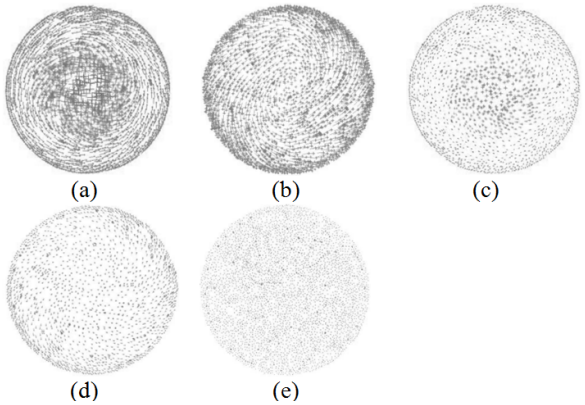

Fig. 3 (a) v_p at pipe inlet section, (b) v_p at pipe exit section at t_p=1 mm, (c) v_p at pipe exit section at t_p=3mm, (d) v_p at pipe exit section at t_p=6mm and (e) v_p at pipe exit section at t_p=12mm

The effect of plate thickness on the swirl angle and tangential velocity is illustrated in Fig. 4. The tangential velocity is more affected by the plate thickness than swirl angle. However, both decrease significantly when the plate thickness increases.

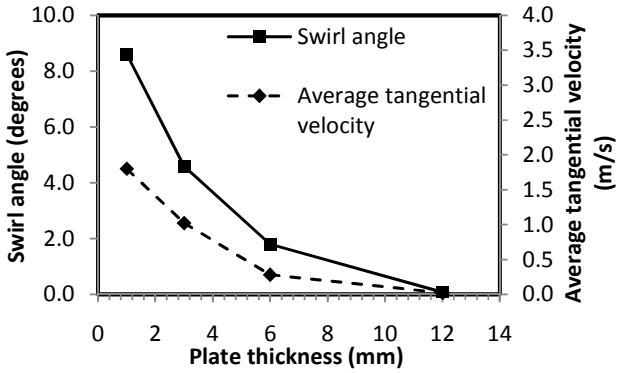

Fig. 4 Average tangential velocity and swirl angle at pipe outlet for different plate thicknesses

Compared to the flow pattern, the increase in plate thickness was found to increase the pressure drop across the circle grids space filling flow conditioner by only 16%, which is relatively insignificant. At the maximum plate thickness, the pressure drop was found to be 276.36 Pa, compared to 238.5 Pa at the standard thickness. The reason behind is that pressure drop is highly dependent on the boundary layer behavior, and in the present case, the plate thickness, even at maximum value, does not allow the boundary layer to uniformly develop in the plate holes. As for the tangential velocity, the smaller

diameter holes near the boundary flow region modify the tangential velocity, which has higher values near the walls, and turn it into axial velocity. That is why the axial velocity increases at the exit plane.

VI. Conclusion

A 3-D numerical investigation of the incompressible isothermal flow through the circle grids space filling plate has been conducted. The CFD model was validated through comparison with the ISO pressure drop correlation. The comparison showed that realizable k-ε turbulence model yielded better agreement than other examined models for the available computing resources. A detailed description of the flow field through the plate has been presented. A flow conditioning effect has been revealed through the flow insight. The plate thickness was found to have a fundamental effect on the flow quality in terms of swirl removal. Plate thickness was proved to be inversely proportional to the swirl angle and tangential velocity component. The average tangential velocity at the outlet plane decreased from 4.8 m/s to 0.06 m/s when the plate thickness increased from 1 mm to 12 mm, respectively, at the same inlet conditions. As for the swirl angle, it decreased from 8.8^{o} to 0.06^{o} due to the same increase in plate thickness. The study suggests that circle grids space filling plate can be employed as a conditioner with optimized plate thickness.

Acknowledgment

Partial support was provided by MOHE (Ministry of Higher Education, MALAYSIA) under Fundamental Research Grant Scheme, vote 1056.

References

[1] Aichouni, M., Laws, E. M., and Ouazzane, A. K., 'Experimental study of the effects of upstream flow condition upon venturi flow meter performance'., In Flow Modelling and Turbulence Measurements VI, pp. 209-216, (1996)

[2] Aichouni, M., Mous, M., Benchicou, S., Mouaici, M., Belghit, M., and Mechmeche, M., 'How flowmeter condition affects measurements accuracy', Proceeding of the 7th International Symposium on Flow Modelling and Turbulence Measurements, Tainan, Taiwan, October 5 - 7. (1994)

[3] [3] Yeh, T. T., and Mattingly, G. E., 'Flow meter installation effects due to a generic header', NIST Technical note 1419. (1996)

[4] ISO 5167:2003, 'Measurement of fluid flow by means of pressure differential devices inserted in circular cross-section conduits running full.' (2003)

[5] Quazzane AK, Benhadj R (2002). Flow Conditioners Design and Their Effects in Reducing Flow Metering Errors. *Sensor Review* 22(3):223–231

[6] Baker RC (2000). *Flow Measurement Handbook: Industrial Designs, Operating Principles, Performance and Applications*, Cambridge University Press, 27–30.

[7] Manshoor B., Nicolleau, F. C. G. A., and Beck, S. B. M., 'The fractal flow conditioner for orifice plate flow meters', Flow Measurement and Instrumentation, 2011. 22(3): p. 208-214. (2011)

[8] Fluent Inc. (2005). *FLUENT 6.2 User's Guide*, 2005-01-04.

[9] Launder BE, Spalding DB (1972). *Lectures in Mathematical Models of Turbulence*. Academic Press, London, England.

[10] Shih TH, Liou WW, Shabbir A, Yang Z, Zhu J (1995). A New k-ε Eddy-Viscosity Model for High Reynolds Number Turbulent Flows - Model Development and Validation. *Computers and Fluids* 24(3):227–238.

[11] Gibson MM, Launder BE (1978). Ground Effects on Pressure Fluctuations in the Atmospheric Boundary Layer. *J. Fluid Mech.* (86):491–511.

[12] Launder BE (1989). Second-Moment Closure: Present... and Future? *International Journal of Heat and Fluid Flow* 10(4):282–300.